Numerical study of magnetization plateaus in the spin-$\frac{1}{2}$ Heisenberg antiferromagnet on the checkerboard lattice

Sylvain Capponi*

Laboratoire de Physique Théorique, IRSAMC, Université de Toulouse, CNRS, F-31062, Toulouse, France and Department of Physics, Boston University, 590 Commonwealth Avenue, Boston, Massachusetts 02215, USA

(Received 16 November 2016; revised manuscript received 3 January 2017; published 18 January 2017)

We present numerical evidence that the spin-1/2 Heisenberg model on the two-dimensional checkerboard lattice exhibits several magnetization plateaus for $m = 0$, 1/4, 1/2, and 3/4, where m is the magnetization normalized by its saturation value. These incompressible states correspond to somewhat similar valence-bond crystal phases that break lattice symmetries, though they are different from the already established plaquette phase for $m = 0$. Our results are based on exact diagonalization as well as density-matrix renormalization-group large-scale simulations and interpreted in terms of simple parameter-free trial wave functions.

DOI: 10.1103/PhysRevB.95.014420

I. INTRODUCTION

Corner-sharing lattices, such as kagomé or checkerboard ones in two dimensions and hyperkagomé and pyrochlore lattices in three dimensions, are known to be ideal playgrounds for study of geometrical frustration. At the classical level, the Heisenberg model can we rewritten up to a constant as

$$\mathcal{H} = J \sum_{\langle ij \rangle} \boldsymbol{S}_i \cdot \boldsymbol{S}_j = \frac{J}{2} \sum_{\text{simplex } \alpha} \boldsymbol{S}_\alpha^2 + \text{Cst}, \tag{1}$$

where the second sum runs over all simplexes (triangles or tetrahedra) α and $J > 0$ is the antiferromagnetic exchange. Thus, classical configurations must satisfy a local constraint $\boldsymbol{S}_\alpha = 0$, $\forall \alpha$, which implies a continuous degeneracy and an extensive entropy. This is the paradigmatic example of magnetic frustration leading to a disordered state for all temperatures [1]. Some famous examples are found in the three-dimensional pyrochlore lattice [2,3], which can be realized in several materials [4]. Henceforth, we concentrate on the two-dimensional analog, known as the checkerboard lattice (see Fig. 1), which is a square lattice of tetrahedra and thus more amenable to numerical simulations.

One expects on general grounds that quantum fluctuations will select some configurations among this manifold (the so-called order-by-disorder phenomenon [5]). Indeed, spin-wave calculations have shown that the magnetically ordered Néel state is unstable towards a paramagnetic one for any spin S [6]. Early numerical studies on the $S = 1/2$ Heisenberg model pointed towards a nonmagnetic state with a large spin gap [7] (i.e., a plateau for zero magnetization), corresponding to some plaquette ordering [8–11]. In principle, other (more exotic) phases are also possible when considering different couplings, inter- and intratetrahedra and anisotropic, along the two axes [10,12–15].

In the presence of a magnetic field h, the Hamiltonian is simply changed to include a Zeeman term:

$$\mathcal{H} = J \sum_{\langle ij \rangle} \boldsymbol{S}_i \cdot \boldsymbol{S}_j - h \sum_i S_i^z. \tag{2}$$

We fix $J = 1$ as the unit of energy in the following. For such a frustrated system, one generically expects magnetization plateaus to appear in the magnetization curve. This is simply because at the classical level, for instance, the system remains very frustrated so that the situation is analogous to the zero-field case. For example, in the classical XY case, thermal fluctuations will select some $\uparrow\uparrow\uparrow\downarrow$ state, thus leading to a plateau at $m = 1/2$ (the magnetization $m = 2\langle \sum_i S_i^z \rangle / N$, where N is the number of sites, is normalized to its saturation value 1) [16]. The same plateau can also be stabilized in the classical Heisenberg model on a three-dimensional analogous pyrochlore lattice when spins are coupled to the lattice [17]. A similar mechanism can also occur in the quantum case: as an example, let us mention recent studies on the spin-1/2 Heisenberg model on a kagomé lattice, where magnetization plateaus corresponding to incompressible phases that break lattice symmetries, so-called valence-bond crystal (VBC) states, have been established numerically for $m = 1/3$, 5/9, and 7/9 in Refs. [18] and [19].

Another clue that plateaus may appear is provided via an *exact localized magnon state* that can be constructed close to the saturation field on such lattices [20]. For the checkerboard lattice, one thus expects [21,22] a plateau at $m = 3/4$, corresponding to a fourfold degenerate VBC with a finite gap to all excitations.

Let us remember also that a commensurability criterion has to be satisfied in one dimension [23], which was also generalized to any dimension [24]: a unique featureless gapped state is possible iff $nS(1 - m) \in \mathbb{Z}$, where n is the number of sites in the unit cell, i.e., $n = 2$ for the checkerboard lattice. Therefore, any plateau at finite $0 < m < 1$ must correspond either to a VBC with a larger unit cell, $n > 2$, or to a topological state. Clearly the latter possibility is an exciting one, and indeed it was suggested for the $m = 1/9$ plateau on a kagomé lattice [19]. On the checkerboard lattice, our study will provide numerical evidence for several plateaus, at $m = 0$, 1/4, 1/2, and 3/4, all of which correspond to VBC phases that are either twofold or fourfold degenerate, depending on m.

Let us mention that similar results were recently reported [25] using density-matrix renormalization-group (DMRG) computations and are discussed accordingly in Sec. III.

*capponi@irsamc.ups-tlse.fr

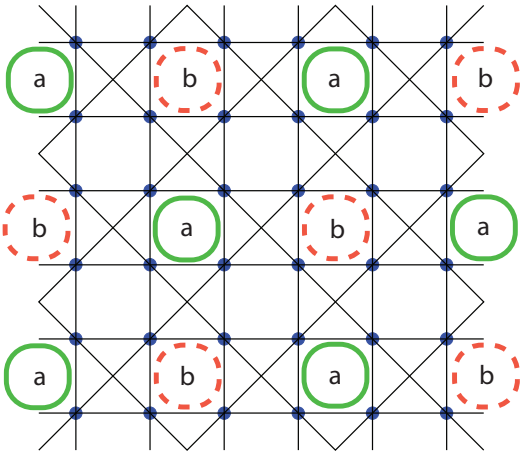

FIG. 1. Sketch of the VBC phase, where a and b denote eigenstates of a plaquette with total spin a and b, respectively. For instance, the product state obtained with $(a,b) = (1,2)$ is an exact ground state [26] for $m = 3/4$. We argue that similar phases with $(0,1)$ and $(0,2)$ are also realized for $m = 1/4$ and $1/2$, respectively. In the $m = 0$ case, the ground state can be understood using the $(0,0)$ product state [8,9,11].

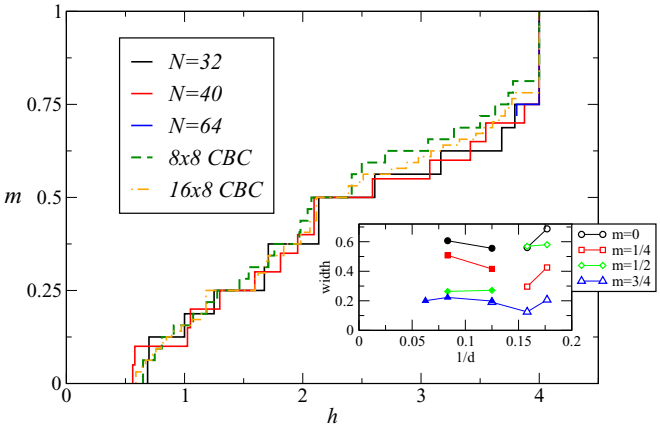

FIG. 2. Magnetization curves of the $S = 1/2$ Heisenberg model on the checkerboard lattice for clusters that can accommodate the VBC shown in Fig. 1 for all interesting m. Solid lines correspond to ED with periodic boundary conditions, and dashed lines to DMRG with CBC; see text. Inset: Widths of the $m = 0$, $1/4$, $1/2$, and $3/4$ plateaus obtained from ED (open symbols) and DMRG (filled symbols) on various clusters, plotted as a function of the inverse diameter. Data are consistent with finite values for all plateaus in the thermodynamic limit.

The outline of this paper is as follows: we provide simple variational states that describe the various VBCs in Sec. II together with exact diagonalization results. Then, in Sec. III, we present large-scale DMRG data as well as an extension to spin anisotropic interaction. A discussion and conclusion are given in Sec. IV.

II. VARIATIONAL STATES AND EXACT DIAGONALIZATION STUDY

A. Magnetization curves

We have performed extensive exact diagonalization (ED) using the Lanczos algorithm in order to compute the magnetization curve for various lattices using periodic boundary conditions to minimize finite-size effects. Basically, one simply needs to compute the total ground-state energy vs the total spin $S_z^{\rm tot}$ (without any magnetic field h) and then perform a Legendre transform to obtain $m(h)$.

As mentioned, exact localized ground states can be built at $m = 3/4$, and they correspond to the pattern shown in Fig. 1 (see Ref. [26]), which possesses an eight-site unit cell. As a consequence, we have chosen clusters that can accommodate such a VBC, such as $N = 32$ (which has additional symmetry [8]), $N = 40$, and $N = 64$. This localized magnon state corresponds to

$$|\Psi_{\rm VBC}^{3/4}\rangle = \prod_j |L,\downarrow\rangle_j \prod_\ell |\uparrow\rangle_\ell, \tag{3}$$

where the first product runs over an ordered pattern of all nonoverlapping squares denoted a in Fig. 1 and the second product runs over the remaining, b sites. The localized-magnon state on a square is the ground state with a single spin-down. Therefore, this exact VBC state can be viewed as a product state using the $S_\square = 1$ ground state on a plaquettes and $S_\square = 2$ (i.e., polarized state) on b ones. We denote this product state $(a,b) = (1,2)$.

Similarly, to what we have observed on the kagomé lattice [18], we may construct similar product-state variational wave functions by simply flipping more spins on the a or b plaquettes, hence getting a trial wave function at $m = 1/2$ corresponding to $(0,2)$ or even $m = 1/4$ for $(0,1)$. Of course, these are no longer exact eigenstates, and nothing guarantees that they have any physical meaning for our microscopic model. So let us now present our unbiased numerical data. It is noteworthy that product-state wave functions can naturally appear to describe some one-dimensional plateaus too [27].

In Fig. 2, we plot the magnetization curve obtained on our particular choice of clusters, thus extending data published in Ref. [26]. First, we recover some known features, such as the finite spin gap ($m = 0$ plateau), estimated at $\Delta \simeq 0.6J$ previously [8,11], as well as the exact saturation field, $h = 4J$, which can be understood in terms of the localized magnon eigenstates and a jump to $m = 3/4$. Moreover, we observe several finite-size plateaus, including rather large ones for $m = 1/2$ and $m = 1/4$. A finite-size analysis for these values is performed in Fig. 2 but it is rather difficult to draw conclusions about the thermodynamic stability, especially for $m = 1/4$. However, general arguments require that the $m = 3/4$ plateau should be finite [21,22] and we remind the reader that the spin gap (i.e., plateau for $m = 0$) is believed to be finite from the literature (see above).

B. Energy spectroscopy from exact diagonalization

Moreover, we can gain additional spectral signatures of these plateaus from ED data on low-energy-level excitations. More specifically, possible symmetry breaking can be investigated using the low-energy levels labeled by their quantum numbers. Since we are using periodic boundary conditions, we can label each eigenstate with magnetization S^z and with its momentum, plus, when allowed, the irrep of the point-group

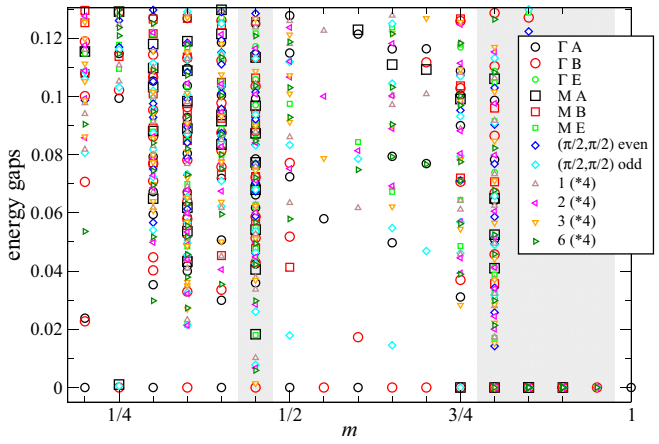

FIG. 3. Energy gaps vs m for $N = 40$ lattice labeled with their quantum numbers. Relevant momenta are labeled as $\Gamma = (0,0)$, $M = (\pi,0)$ and 2-fold degenerate $(\pi/2,\pi/2)$. For $m = 1/4$, $1/2$ and $3/4$, the lowest states correspond to the expected four ones in the Brillouin zone. The magnetization sectors with a gray background are not visited in the magnetization curve, i.e., they are obscured by a magnetization jump.

symmetry. Note that we use the square-lattice Brillouin zone, which has to be folded for a checkerboard lattice with two-site unit cell.

For the proposed fourfold degenerate VBC states at finite m, a symmetry analysis leads to four degenerate states: one at the Γ point, one at $M = (\pi,0)$, and one at each (twofold degenerate) $(\pi/2,\pi/2)$ momentum. In Fig. 3, we plot the energy gaps for each magnetization sector on an $N = 40$ cluster, and we do observe a very good (quasi-)degeneracy of these four states and a sizable gap above for $m = 1/4$ and $m = 3/4$. At $m = 1/2$, these are also the lowest states but the separation is less clear, presumably due to the larger correlation length.

C. Correlations

Another piece of evidence comes from the computation of specific correlations using the unique finite-size ground state. More specifically, for each magnetization m, we have computed connected spin correlation functions

$$\langle S_i^z S_j^z \rangle_c = \langle S_i^z S_j^z \rangle - \langle S_i^z \rangle \langle S_j^z \rangle \tag{4}$$

as well as connected dimer-dimer correlations

$$\langle (\boldsymbol{S}_i \cdot \boldsymbol{S}_j)(\boldsymbol{S}_k \cdot \boldsymbol{S}_\ell) \rangle_c = \langle (\boldsymbol{S}_i \cdot \boldsymbol{S}_j)(\boldsymbol{S}_k \cdot \boldsymbol{S}_\ell) \rangle - \langle (\boldsymbol{S}_i \cdot \boldsymbol{S}_j) \rangle \langle (\boldsymbol{S}_k \cdot \boldsymbol{S}_\ell) \rangle \tag{5}$$

using ED on various lattices.

Similarly to what was done on the kagomé lattice [18], one can obtain an exact expression for the $m = 3/4$ VBC state [see Fig. 1 or Eq. (3)]. Discarding short-distance data that require a separate calculation, one can easily get that (i) the average $\langle \boldsymbol{S}_i \cdot \boldsymbol{S}_j \rangle = 1/16$; (ii) connected correlations between "strong" plaquette bonds are $9/256 \simeq 0.035$; and (iii) connected correlations between strong and weak plaquette bonds are $-7/256 \simeq -0.027$. These are exactly the numbers we get in Fig. 4 (with small deviations due to the finite overlap of the four localized magnon states in a finite cluster). A similar calculation can be performed for any trial state (a,b), and in Fig. 4 we compare ED data to the simple VBC, respectively, given as $(a,b) = (0,0)$ for $m = 0$, $(0,1)$ for $m = 1/4$, $(0,2)$ for $m = 1/2$, and $(1,2)$ for $m = 3/4$. In all cases, we do observe a (semi-)quantitative agreement, which strongly supports the description of all these plateau states in terms of the simple VBC as sketched in Fig. 1.

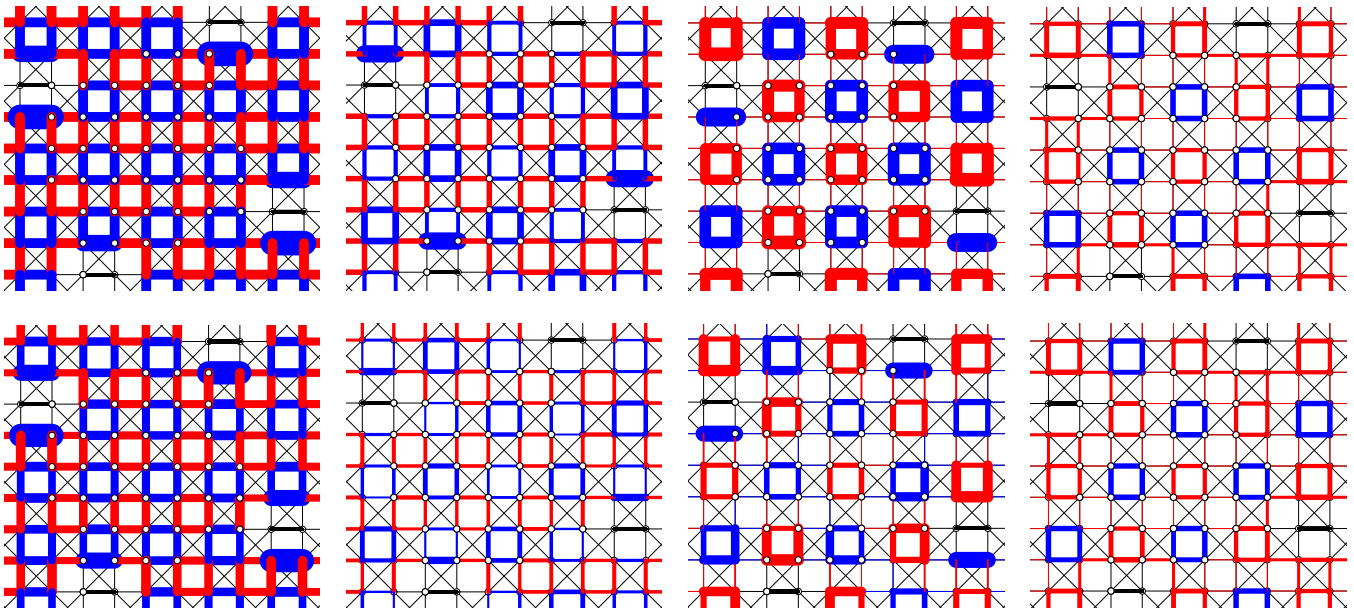

FIG. 4. Dimer-dimer correlations [cf. Eq. (5)] computed on an $N = 40$ cluster: positive and negative values are shown by blue and red lines, respectively, and the width is proportional to the data; the reference bond is shown in black. From left to right, data correspond to the ground state for $m = 0$, $1/4$, $1/2$, and $3/4$. The top row corresponds to simple VBC states where computation is done analytically without any free parameter (see text); the bottom row corresponds to ED results for the Heisenberg model.

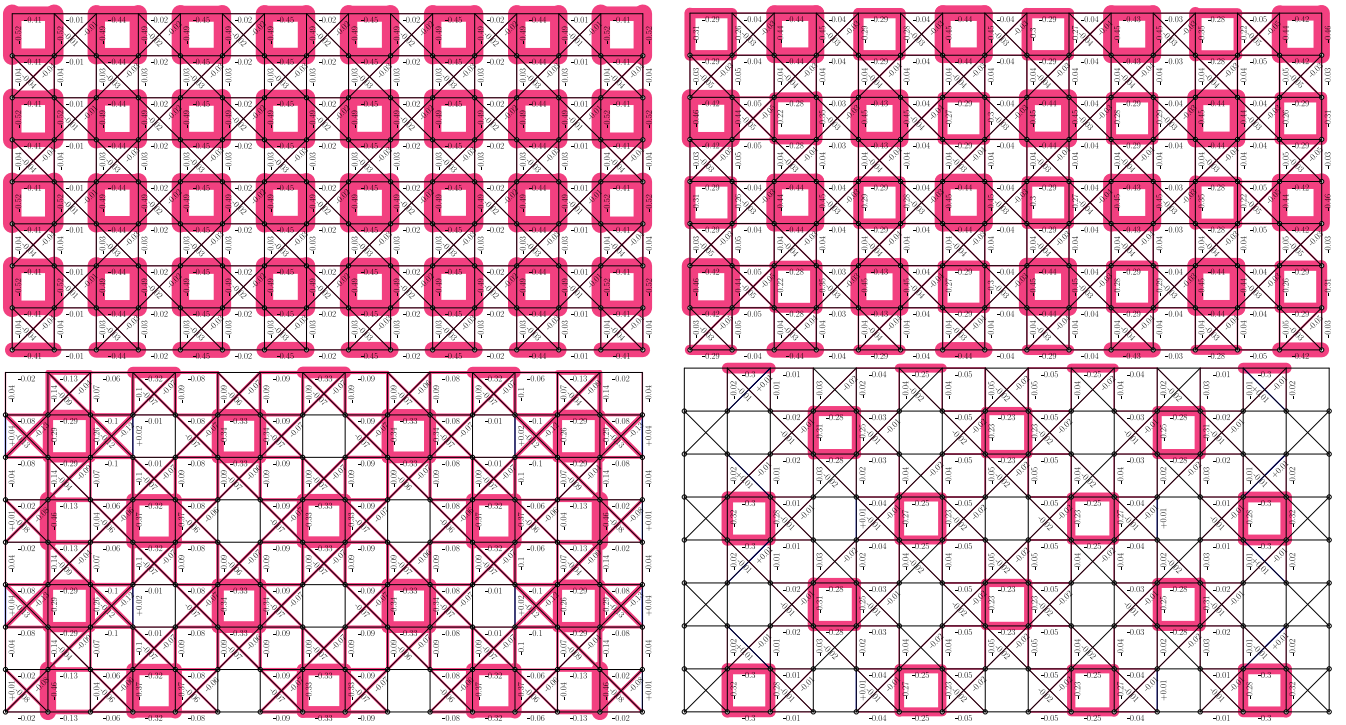

FIG. 5. Bond strengths for $m = 0$, $m = 1/4$, $m = 1/2$, and $m = 3/4$ (from top to bottom and left to right) on a 16×8 cylinder using DMRG simulations and keeping up to 6000 states. In each plot, the top and bottom lines are identical due to periodic boundary conditions along this direction (CBC). Data larger than 0.01 (in absolute value) are written in the plot.

III. DMRG RESULTS

A. Simulations on large cylinders

We now turn to large-scale simulations using the two-dimensional DMRG algorithm [28], which can be applied to cylinders provided that the width is not too large. We have kept up to $m = 6000$ states in order to obtain a good convergence of our results and a small discarded weight. We use cylindrical boundary conditions (CBCs).

In Fig. 2, we have plotted the magnetization curve on a few cylinders which exhibit large plateaus for the expected magnetizations. Note that the $m = 3/4$ plateau is slightly shifted due to boundary effects, so that we have systematically taken the plateau next to the jump to saturation instead (which converged to $3/4$ in the thermodynamic limit). A finite-size scaling can be performed to check that all four proposed VBCs are stable in the thermodynamic limit; see the inset in Fig. 2, with data obtained on 12×8, 16×12, and 16×16 cylinders.

In Fig. 5, we plot the local bond strengths $\langle \boldsymbol{S}_i \cdot \boldsymbol{S}_j \rangle - \langle S_i^z \rangle \langle S_j^z \rangle$ for various magnetizations. Data are compatible with a fourfold degenerate ground state at $m = 1/4$, $m = 1/2$, and $m = 3/4$ but only twofold for $m = 0$, as expected from our trial wave-function guess. We remind the reader that the DMRG algorithm will target one particular VBC, and not a superposition, since it converges to so-called minimally entangled states [29]. In addition, while for $m = 0$, all sites have a vanishing magnetization on average ($\langle S_i^z \rangle = 0 \, \forall i$), which is an exact result [30], we have found a clear modulation in this quantity for all $m > 0$ plateaus states, in agreement with the proposed VBC states. More precisely, for the plateaus corresponding to $m = 1/4$, $1/2$, and $3/4$, we have argued that they could be understood using simple product states with total spin a and b on alternating four-site plaquettes. Respectively, we have proposed $(a,b) = (0,1)$, $(0,2)$, and $(1,2)$ (see Fig. 1). So in principle, using a DMRG simulation on cylinders that target one particular state, *we can directly measure the local magnetization* $\langle S_i^z \rangle$ to characterize the state. This is shown in Fig. 6 for a 16×8 cylinder. In all cases, the total magnetization on each four-site plaquette is very close to the expected one in a simple product state, i.e., $S_{\square}^z = 0$, 1, or 2. We note also that there are strong edge effects so one should be cautious with boundary conditions and extrapolations. This is also why, for instance, we have fixed $m = 3/4 + 2/N$, where N is the number of sites, so that the bulk resembles more the genuine $m = 3/4$ ground state.

Similar results for the bond pattern and the local magnetizations were obtained in Ref. [25] using the DMRG as well, but with modified boundary conditions to minimize finite-size effects, at the cost of having to fix the magnetic field and not the total magnetization (grand-canonical approach). Both studies agree on the existence and nature of the plateau phases at $m = 0$, 1/4, 1/2, and 3/4. Moreover, Morita and Shibata argue in favor of a small plateau at $m = 3/8$ and maybe also at $m = 1/8$, where they observe a small anomaly.

B. Quantum phase transition away from the SU(2) case

In order to make connections with related strongly correlated models on the same lattice, it proves useful to investigate

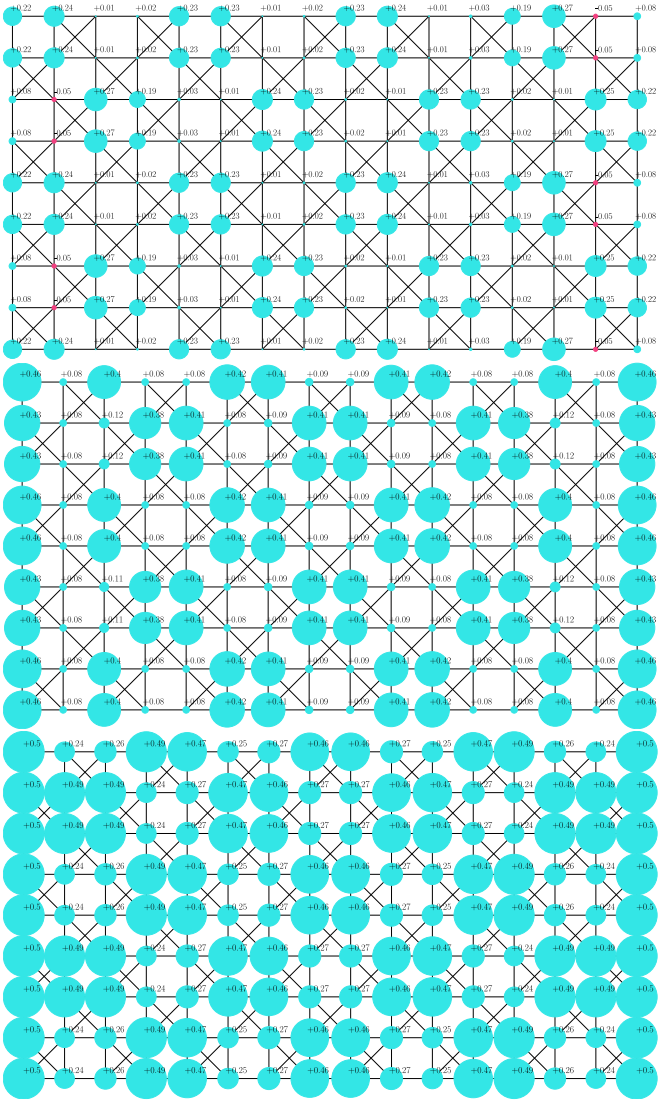

FIG. 6. Local magnetization for $m = 1/4$, $m = 1/2$, and $m = 3/4$ (from top to bottom) on a 16×8 cylinder using DMRG simulations and keeping up to 6000 states. The radius is proportional to the absolute value. Due to edge effects, for the $m = 3/4$ plot, we have used a slightly higher total magnetization ($m = 3/4 + 2/128$) to get a clearer picture of the bulk behavior. Top and bottom lines are identical (CBC).

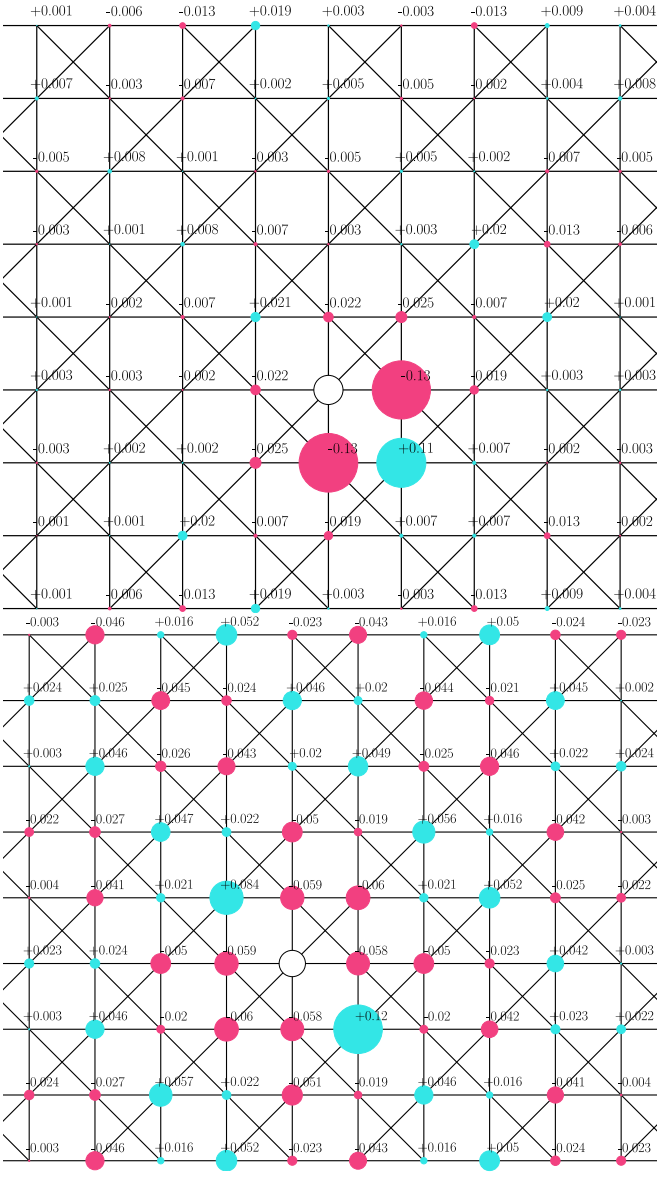

FIG. 7. Connected S^z correlations between the reference site (black circle) and the neighboring ones computed using DMRG at $m = 1/2$ on a 16×8 cylinder using CBC. Top panel, $\Delta = 1$; bottom panel, $\Delta = 5$. Only data within the bulk are shown. Positive and negative values are shown in blue and red, respectively.

the (spin) anisotropic *XXZ* model,

$$\mathcal{H} = \sum_{\text{bonds}\,(i,j)} \frac{1}{2}\left(S_i^+ S_j^- + S_i^- S_j^+\right) + \Delta S_i^z S_j^z, \qquad (6)$$

where Δ quantifies the anisotropy. Here, we focus on the $m = 1/2$ plateau and we show how increasing Δ leads to a quantum phase transition and a qualitative change in the physical properties.

Indeed, for strong $\Delta \gg 1$, the model maps onto a purely kinetic quantum dimer model, which is defined on a new square lattice whose sites are at the center of the crossed plaquettes of the original one. The mapping simply consists of associating a dimer with each down-spin and the hard-core constraints simply reflect the ice rule (one down-spin per crossed plaquette). The quantum dimer model ground state is known to be columnarlike [31–34], so that the ground state is also fourfold degenerate, but of a different kind.

By computing the ground state with $m = 1/2$ at $\Delta = 5$ with the DMRG, we have observed that there are qualitatively distinct features with respect to the SU(2) case ($\Delta = 1$): both local magnetization and bond strengths become uniform in the bulk (data not shown), i.e., no evidence of a simple VBC was found at $\Delta = 1$. To clarify the different nature of these ground states, we plot in Fig. 7 the connected correlations $\langle S_i^z S_j^z\rangle - \langle S_i^z\rangle\langle S_j^z\rangle$ in both regimes. For $\Delta = 1$, we have previously shown that the ground state is a VBC with inhomogeneous sites)see Fig. 6), so that in principle we

would need to compute different correlations depending on the reference site. However, this is for illustration only since we already know the nature of this VBC and these correlation data simply reflect that we have a low-entangled state, close to a product-state, so that correlations between plaquettes are very small, and inside one plaquette, they show the expected pattern for (here) a singlet state. On the contrary, for $\Delta = 5$, Fig. 7 provides strong evidence that the ground-state at $m = 1/2$ is similar to the columnar phase of the effective quantum dimer model: in spin language, we have diagonal lines that repeat a simple $\downarrow\uparrow\uparrow\uparrow$ pattern, thus explaining the observed pattern. So in spin language, it corresponds to a ferrimagnetic phase, not a VBC one.

IV. CONCLUSION

We have provided strong numerical evidence in favor of the existence of magnetization plateaus in the spin-1/2 Heisenberg model on a two-dimensional checkerboard lattice for $m = 0$, $1/4$, $1/2$, and $3/4$ of its saturation value. While the $m = 0$ plateau (due to the finite spin gap) was previously known from the literature [6–11] and corresponds to a twofold degenerate VBC, we find that the three others are well described by a fourfold degenerate VBC, analogous to the exact localized magnon eigenstate that can be constructed at $m = 3/4$ [26]. Thus, the situation is rather similar to another famous corner-sharing geometry, namely, the kagomé lattice, where the same phenomenology was recently observed [18,19]. It seems that the finite-field situation can be better understood from the large-field limit, which is presumably more amenable to theoretical techniques, or less frustrated in a sense. Moreover, these product states can also be interpreted as having quantized spin imbalance (obtained by measuring magnetization in different blocks), which could be interpreted as a remnant of the classical degeneracy through an order-by-disorder mechanism [27].

We would also like to comment on the adiabatic connections (or not) between these plateau phases and similar ones that have been observed in different contexts [35]. For $m = 0$, there is recent numerical evidence of the plaquette phase persisting in the antiferromagnetic XY limit [36]. In the opposite XXZ limit with dominant Ising interaction, the $m = 0$ and $m = 1/2$ low-energy configurations can be easily seen to be in one-to-one correspondence with the quantum loop [37] and quantum dimer configurations on a square lattice, respectively. Both effective constrained models are of the Rokhsar-Kivelson type [38], with purely kinetic terms, and have been investigated quite extensively. This quantum loop model (also known as square ice) has a twofold degenerate plaquette ground state [37,39], i.e., a structure similar to that of our (0,0) product state, hence pointing to a robust feature present for any anisotropy in the XXZ sense. On the contrary, the quantum dimer model with purely kinetic terms has a fourfold degenerate columnar ground state [40], which, when translated into spin language, would correspond to a ferrimagnetic state with fixed local magnetization $\pm 1/2$, i.e., qualitatively different from the resonating state that we have found in the SU(2) case. Therefore, we predict the existence of a quantum phase transition when increasing the anisotropy of the XXZ model between a VBC and an ordered ferrimagnetic phase, which is confirmed numerically (see Sec. III B). The nature of this phase transition is potentially interesting (continuous vs first order; see, for instance, Ref. [41]) but a complete analysis is postponed to a future study. In a similar manner, it would be natural to investigate the fate of $m = 1/4$ and $3/4$ plateaus when moving away from the SU(2) case. In addition, it would be interesting to prove whether supersolidity can be stabilized in the vicinity of some of these plateaus, a phenomenon which is common on frustrated lattices but not present on the checkerboard lattice for interacting hard-core bosons with nonfrustrated hopping [42].

As far as fermionic Hubbard-like models on the same lattice are concerned, it has been shown that various VBCs can also be stabilized at commensurate fillings [43–45]. Generalization of spin models with SU(N) symmetry (using a fundamental representation at each site) can also host other kinds of valence-bond solid states [46]. Hence, a global picture of the effect of strong quantum correlations is emerging thanks to all of these studies and provides new exotic phases compared to the classical ones.

Note added. During the completion of this work, a related DMRG study appeared [25] that fully agrees on the nature and stability of the proposed VBCs here.

ACKNOWLEDGMENTS

This work was performed using HPC resources from GENCI (Grants No. x2015050225 and No. x2016050225) and CALMIP. The author thanks Institut Universitaire de France (IUF) for funding when this work started and the Condensed Matter Theory Visitors Program at Boston University for financial support during the completion of the manuscript. Discussions with Andreas Läuchli and Xavier Plat are acknowledged.

[1] J. Villain, Z. Phys. B **33**, 31 (1979).
[2] J. N. Reimers, Phys. Rev. B **45**, 7287 (1992).
[3] R. Moessner and J. T. Chalker, Phys. Rev. Lett. **80**, 2929 (1998).
[4] J. S. Gardner, M. J. P. Gingras, and J. E. Greedan, Rev. Mod. Phys. **82**, 53 (2010).
[5] J. Villain, R. Bidaux, J.-P. Carton, and R. Conte, J. Phys. **41**, 1263 (1980).
[6] B. Canals, Phys. Rev. B **65**, 184408 (2002).
[7] S. E. Palmer and J. T. Chalker, Phys. Rev. B **64**, 094412 (2001).
[8] J.-B. Fouet, M. Mambrini, P. Sindzingre, and C. Lhuillier, Phys. Rev. B **67**, 054411 (2003).
[9] W. Brenig and A. Honecker, Phys. Rev. B **65**, 140407 (2002).
[10] O. Tchernyshyov, O. A. Starykh, R. Moessner, and A. G. Abanov, Phys. Rev. B **68**, 144422 (2003).
[11] E. Berg, E. Altman, and A. Auerbach, Phys. Rev. Lett. **90**, 147204 (2003).
[12] J.-S. Bernier, C.-H. Chung, Y. B. Kim, and S. Sachdev, Phys. Rev. B **69**, 214427 (2004).

[13] O. A. Starykh, A. Furusaki, and L. Balents, Phys. Rev. B **72**, 094416 (2005).
[14] S. Moukouri, Phys. Rev. B **77**, 052408 (2008).
[15] Y.-H. Chan, Y.-J. Han, and L.-M. Duan, Phys. Rev. B **84**, 224407 (2011).
[16] B. Canals and M. Zhitomirsky, J. Phys.: Condens. Matter **16**, S759 (2004).
[17] K. Penc, N. Shannon, and H. Shiba, Phys. Rev. Lett. **93**, 197203 (2004).
[18] S. Capponi, O. Derzhko, A. Honecker, A. M. Läuchli, and J. Richter, Phys. Rev. B **88**, 144416 (2013).
[19] S. Nishimoto, N. Shibata, and C. Hotta, Nat. Commun. **4**, 2287 (2013).
[20] For a review, see Ref. [26] and references therein.
[21] T. Momoi and K. Totsuka, Phys. Rev. B **61**, 3231 (2000).
[22] M. Oshikawa, Phys. Rev. Lett. **84**, 1535 (2000).
[23] M. Oshikawa, M. Yamanaka, and I. Affleck, Phys. Rev. Lett. **78**, 1984 (1997).
[24] M. B. Hastings, Phys. Rev. B **69**, 104431 (2004).
[25] K. Morita and N. Shibata, Phys. Rev. B **94**, 140404(R) (2016).
[26] J. Richter, J. Schulenburg, A. Honecker, J. Schnack, and H.-J. Schmidt, J. Phys.: Condens. Matter **16**, S779 (2004).
[27] X. Plat, Y. Fuji, S. Capponi, and P. Pujol, Phys. Rev. B **91**, 064411 (2015).
[28] S. R. White, Phys. Rev. Lett. **69**, 2863 (1992).
[29] H.-C. Jiang, Z. Wang, and L. Balents, Nat. Phys. **8**, 902 (2012).
[30] E. H. Lieb and P. Schupp, Phys. Rev. Lett. **83**, 5362 (1999).
[31] O. F. Syljuåsen, Phys. Rev. B **73**, 245105 (2006).
[32] D. Banerjee, M. Bögli, C. P. Hofmann, F.-J. Jiang, P. Widmer, and U.-J. Wiese, Phys. Rev. B **90**, 245143 (2014).
[33] D. Schwandt, S. V. Isakov, S. Capponi, R. Moessner, and A. M. Läuchli (unpublished).
[34] D. Banerjee, M. Bögli, C. P. Hofmann, F.-J. Jiang, P. Widmer, and U.-J. Wiese, Phys. Rev. B **94**, 115120 (2016).
[35] This was, for instance, recently investigated for the kagomé lattice [47,48].
[36] A. M. Läuchli and R. Moessner, arXiv:1504.04380.
[37] N. Shannon, G. Misguich, and K. Penc, Phys. Rev. B **69**, 220403 (2004).
[38] D. S. Rokhsar and S. A. Kivelson, Phys. Rev. Lett. **61**, 2376 (1988).
[39] D. Banerjee, F.-J. Jiang, P. Widmer, and U.-J. Wiese, J. Stat. Mech.: Theory Exp. (2013) P12010.
[40] Let us emphasize that the complete phase diagram of the quantum dimer model on the square lattice is still an ongoing investigation; see Refs. [31–34] and references therein.
[41] J. D'Emidio and R. K. Kaul, arXiv:1610.07702 [cond-mat.str-el].
[42] S. Wessel, Phys. Rev. B **86**, 140501 (2012).
[43] M. Indergand, A. Läuchli, S. Capponi, and M. Sigrist, Phys. Rev. B **74**, 064429 (2006).
[44] M. Indergand, C. Honerkamp, A. Läuchli, D. Poilblanc, and M. Sigrist, Phys. Rev. B **75**, 045105 (2007).
[45] D. Poilblanc, Phys. Rev. B **76**, 115104 (2007).
[46] P. Corboz, K. Penc, F. Mila, and A. M. Läuchli, Phys. Rev. B **86**, 041106 (2012).
[47] D. Huerga, S. Capponi, J. Dukelsky, and G. Ortiz, Phys. Rev. B **94**, 165124 (2016).
[48] A. Kshetrimayum, T. Picot, R. Orús, and D. Poilblanc, Phys. Rev. B **94**, 235146 (2016).